

2018

New constraints on coseismic slip during southern Cascadia subduction zone earthquakes over the past 4600 years implied by tsunami deposits and marine turbidites

GR Priest

RC Witter

Yinglong J. Zhang
Virginia Institute of Marine Science

C Goldfinger

KL Wang

See next page for additional authors

Follow this and additional works at: <https://scholarworks.wm.edu/vimsarticles>



Part of the [Aquaculture and Fisheries Commons](#)

Recommended Citation

Priest, GR; Witter, RC; Zhang, Yinglong J.; Goldfinger, C; Wang, KL; and Allen, JC, "New constraints on coseismic slip during southern Cascadia subduction zone earthquakes over the past 4600 years implied by tsunami deposits and marine turbidites" (2018). *VIMS Articles*. 734.
<https://scholarworks.wm.edu/vimsarticles/734>

This Article is brought to you for free and open access by the Virginia Institute of Marine Science at W&M ScholarWorks. It has been accepted for inclusion in VIMS Articles by an authorized administrator of W&M ScholarWorks. For more information, please contact scholarworks@wm.edu.

Authors

GR Priest, RC Witter, Yinglong J. Zhang, C Goldfinger, KL Wang, and JC Allen

New constraints on coseismic slip during southern Cascadia subduction zone earthquakes over the past 4600 years implied by tsunami deposits and marine turbidites

George R. Priest¹  · Robert C. Witter² · Yinglong J. Zhang³ ·
Chris Goldfinger⁴ · Kelin Wang⁵ · Jonathan C. Allan¹

Received: 24 August 2016 / Accepted: 8 April 2017 / Published online: 29 April 2017
© Springer Science+Business Media Dordrecht (outside the USA) 2017

Abstract Forecasting earthquake and tsunami hazards along the southern Cascadia subduction zone is complicated by uncertainties in the amount of megathrust fault slip during past ruptures. Here, we estimate slip on hypothetical ruptures of the southern part of the megathrust through comparisons of late Holocene Cascadia earthquake histories derived from tsunami deposits on land and marine turbidites offshore. Bradley Lake in southern Oregon lies ~600 m landward of the shoreline and contains deposits from 12 tsunamis in the past 4600 years. Tsunami simulations that overtop the 6-m-high lake outlet, generated

This paper summarizes new tsunami simulation experiments supplementary to those done by Witter et al. (2012).

✉ George R. Priest
gpriest@yahoo.com;
<http://www.oregongeology.org/tsuclearinghouse/>

Robert C. Witter
rwitter@usgs.gov

Yinglong J. Zhang
yjzhang@vims.edu;
http://www.vims.edu/about/directory/faculty/zhang_yj.php

Chris Goldfinger
gold@oce.orst.edu;
<http://www.coas.oregonstate.edu/index.cfm?fuseaction=content.search&searchtype=people&detail=1&id=540>

Kelin Wang
kwang@nrcan-mcan.gc.ca;
http://cgc.nrcan.gc.ca/dir/index_e.php?id=8400

Jonathan C. Allan
jonathan.allan@dogami.state.us.or

¹ Oregon Department of Geology and Mineral Industries, Newport Coastal Field Office, Newport, OR, USA

² U.S. Geological Survey, Alaska Science Center, Anchorage, AK, USA

by ruptures with most slip south of Cape Blanco, require release of at least as much strain on the megathrust as would accumulate in 430–640 years (>15 – 22 m). Such high slip is inconsistent with global seismic data for a rupture ~ 300 -km long and slip deficits over the past ~ 4700 years on the southern Cascadia subduction zone. Assuming slip deficits accumulated during the time intervals between marine turbidites, up to 8 of 12 tsunami inundations at the lake are predicted from a marine core site 170 km north of the lake (at Hydrate Ridge) compared to 4 of 12 when using a core site ~ 80 km south (at Rogue Apron). Longer time intervals between turbidites at Hydrate Ridge imply larger slip deficits compared to Rogue Apron. The different inundations predicted by the two records suggest that Hydrate Ridge records subduction ruptures that extend past both Rogue Apron and Bradley Lake. We also show how turbidite-based estimates of CSZ rupture length relate to tsunami source scenarios for probabilistic tsunami hazard assessments consistent with lake inundations over the last ~ 4600 years.

Keywords Tsunami · Cascadia subduction zone · Bradley Lake · Earthquake · Paleoseismic data · Turbidites · Fault ruptures

Abbreviations

DOGAMI Oregon Department of Geology and Mineral Industries
CSZ Cascadia subduction zone
MHHW Mean higher high water
NOAA National oceanic and atmospheric administration

1 Introduction

Probabilistic tsunami hazard analysis (PTHA) for locally generated tsunamis is a challenging problem for the Cascadia subduction zone (CSZ). The first step in a PTHA entails construction of a logic tree for local earthquake sources based on modern observations and on late Holocene events inferred from paleoseismic and paleotsunami data. Although no modern observations of large CSZ events exist, historical impacts of the AD1700 Cascadia tsunami on Japan's coast were used to constrain the most likely size of the megathrust source: a M_w 9.0 rupture of the entire Cascadia margin with average fault slip of ~ 19 m (Satake et al. 2003). Offshore, the deposits of turbidity currents triggered by seismic shaking (turbidites) imply a 10,000-year history of CSZ megathrust ruptures that vary in length (Fig. 1a; Goldfinger et al. 2012, 2013b, 2016a). Clues to the relative size of CSZ earthquakes include the thicknesses and relative masses of sandy turbidites (Goldfinger et al. 2012, 2013b), coseismic subsidence inferred from studies of salt marsh soils (Atwater and Hemphill-Haley 1997; Kelsey et al. 2002; Nelson et al. 2008; Witter et al. 2003), and tsunami size inferred from tsunami deposits in coastal marshes and lakes (Kelsey et al. 2005; Witter et al. 2012).

³ Center for Coastal Resources Management, Virginia Institute of Marine Science, Gloucester Point, VA, USA

⁴ Oregon State University, Corvallis, OR, USA

⁵ Geological Survey of Canada, Pacific Geoscience Centre, Sidney, BC, Canada

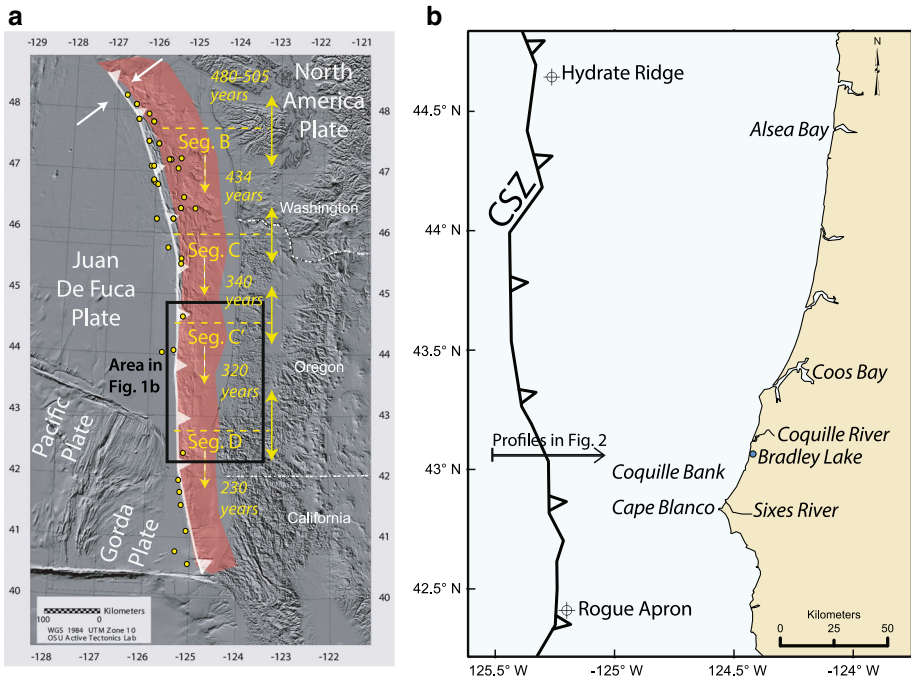


Fig. 1 Location maps. **a** Cascadia subduction zone (CSZ) surface trace (white line with triangles), coseismic rupture area (red) for the full-margin, Segment A ruptures of Goldfinger et al. (2016a). Yellow dashed lines are preferred north boundaries of smaller segment ruptures inferred by Goldfinger et al. (2016a) from turbidite data in marine cores (yellow dots) with uncertainty depicted by yellow arrows; southern boundaries of all segments are at near or the south end of the full-margin rupture area; mean recurrence of CSZ earthquakes between boundaries is from Goldfinger et al. (2016a). White arrows depict general direction of plate convergence. Shade relief map and core locations are from Goldfinger et al. (2016a). **b** Location of geographic features mentioned in the text; circle with cross at Rogue Apron is location of core hole M9907-31PC-TC in the Rogue Canyon channel; circle with cross at Hydrate Ridge is core hole RR0207-56PC-TC

Large uncertainties about the number and geographic extent of past subduction earthquakes on the CSZ, particularly in southern Oregon and northern California (Frankel 2011) further complicate PTHA source characterizations. For example, the 2014 Update to the National Seismic Hazard Maps (Petersen et al. 2014) used a recurrence rate in southern Cascadia of 0.001 per year for M_w 8 southern Cascadia earthquakes, which is about half the rate inferred by Goldfinger et al. (2012) from offshore turbidite history. Debate (Frankel 2011; Atwater et al. 2014; Petersen et al. 2014) over the origin of thin, muddy turbidites found in offshore marine channels and slope basins (Goldfinger et al. 2012, 2013b) has identified the need to reassess the mean rate of earthquake recurrence in southern Cascadia (Petersen et al. 2014). Coastal geology (Kelsey et al. 2005; Nelson et al. 2006; Witter et al. 2012) and marine turbidites (Goldfinger et al. 2013b) imply shorter recurrence intervals in southern Cascadia compared to ruptures that break the entire 1000-km-long Cascadia margin.

Here, we take advantage of tsunami deposits in a southern Oregon coastal lake (Bradley Lake, Kelsey et al. 2005) that offer a unique opportunity to reconstruct tsunami source parameters and estimate the amount of coseismic slip in past great earthquakes (Witter

et al. 2012), including ruptures of the southern part of the CSZ. Bradley Lake lies ~ 600 m landward of the Pacific shoreline and is on the north side of Coquille Bank (Fig. 1b). The lake's history of inundation by CSZ tsunamis extends over the past ~ 4600 years (Kelsey et al. 2005), although disturbances in the lake sediment also record seismic shaking without tsunami inundation. To inundate the lake, tsunamis must overtop the 6-m elevation of the lake outlet, which sets a threshold that prevents inundation by tsunamis with runup < 6 m.

The primary question addressed in this paper is, can constraints on megathrust slip during southern Cascadia earthquakes be improved by using turbidite paleoseismology and coastal tsunami deposits to estimate earthquake and tsunami source parameters for use in PTHA? We address this question by building upon experiments by Witter et al. (2012) who applied fault dislocation and hydrodynamic tsunami models to test whether geologically reasonable rupture models of the southern Cascadia subduction zone are consistent with tsunami deposits found by Kelsey et al. (2005) in Bradley Lake (Fig. 1b). Witter et al. (2012) determined the minimum megathrust slips needed to cause tsunamis to inundate the lake when slip was located directly offshore. For comparison, they estimated coseismic slip during past earthquakes by inferring slip deficit from the time intervals between marine turbidites at the closest high-quality marine core site 80 km south of the lake at Rogue Apron (Fig. 1b). They found that very few slip deficits were large enough to produce enough megathrust slip for the 12 tsunami inundations of the lake during the last ~ 4600 years when coastal physiography was most favorable to inundation. Witter et al. (2012) concluded that slip deficits inferred from time intervals separating earthquake-triggered turbidites are poor predictors of coseismic slip. The simulations performed by Witter et al. (2012) did not include tsunamis generated by partial rupture of the southern Cascadia subduction zone.

Here we expand the Witter et al. source simulation experiments by including ruptures with slip concentrated in the southern ~ 300 km of the CSZ in addition to the previous simulations that used slip concentrated directly offshore of the lake. We test the hypothesis of Priest et al. (2014) that the inefficient projection of tsunami energy from coseismic slip of southern Cascadia ruptures makes this region an unlikely source for tsunamis capable of breaching the 6-m outlet barrier. We also show that simulations are more successful at predicting lake inundation when using coseismic slip estimates derived from turbidite inter-event times excluding events likely caused by CSZ fault ruptures with most slip south of the lake. We then explain how our findings provide guidance on integration of paleoseismic data into a PTHA.

2 Previous tsunami simulations

Witter et al. (2012) performed fault dislocation modeling that predicted sea floor deformation and provided the initial wave forms for tsunami simulations run with the hydrodynamic model, SELFE (Zhang and Baptista 2008) with the assumption of zero bottom friction (Manning coefficient = 0). They developed three full-margin rupture models that varied the slip distribution across the megathrust and, in some cases, diverted slip to a shallow splay fault (Fig. 2). One rupture model distributed slip symmetrically on the megathrust and tapered slip to zero both up and down dip (e.g., Wang and He 2008; Priest et al. 2010). Another model diverted slip to a shallow splay fault by truncating the symmetrical slip distribution of the first model at the surface trace of the splay fault (Fig. 2). A third rupture model skewed megathrust slip seaward (Fig. 2) but produced a poorer fit to

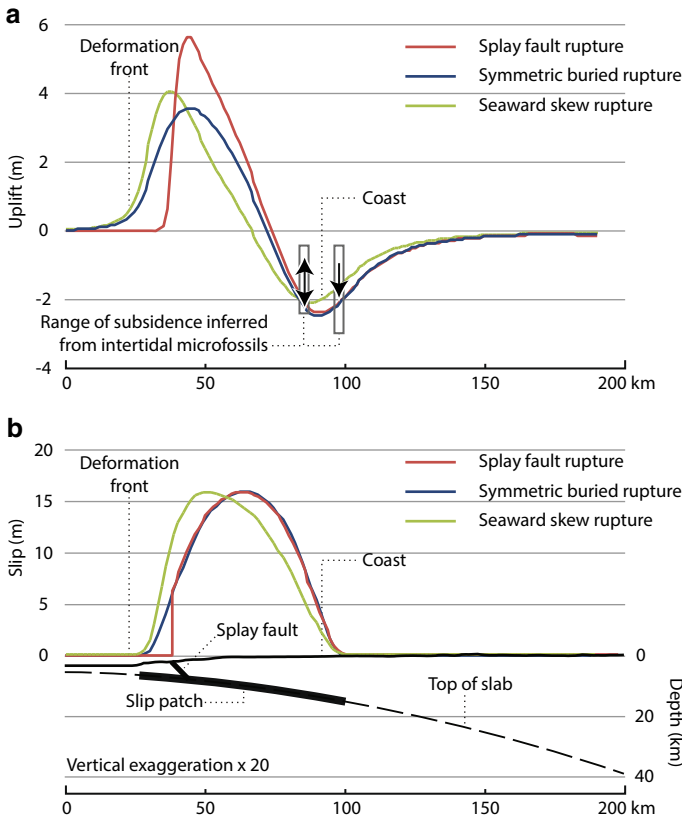


Fig. 2 Cascadia earthquake scenarios of Witter et al. (2012) at the latitude of Bradley Lake. **a** Vertical deformation with rectangles spanning the range of subsidence inferred from fossil diatom assemblages (refs Kelsey et al. 2002; Witter et al. 2003). **b** Profile of fault slip distribution. Red line shows slip truncated where the splay fault intersects the sea floor. Bold black line delineates slip patch on plate interface. Figure taken from Witter et al. (2012). Only the symmetric buried rupture case was utilized to simulate southern Cascadia sources in this study

co-seismic subsidence estimates and created smaller tsunamis than the two principal models (Witter et al. 2012). They found that simulations of the AD1700 tsunami on an AD1700 landscape (Fig. 3) required a minimum of 14–16 m of slip (equivalent to the release of 360–400 years of slip deficit and assuming a fully locked plate boundary) to reach Bradley Lake. The simulation was run with tide at mean sea level (MSL) + 0.5 m (1.55 m NAVD 88); approximating the hindcast tide in AD1700 that included subtidal fluctuations in winter water levels (Mofjeld et al. 1997; Table 1). The smallest earthquake that could cause lake inundation released a minimum inferred slip deficit of 260 and 290 years (10 and 11 m of coseismic slip) and utilized an eroded shoreline landscape (Fig. 3). The range of slips for each of the two landscapes is caused by the larger uplift of the seafloor by the splay fault source relative to the symmetric slip source for a given amount of slip deficit release (Table 1).

The Witter et al. (2012) experiments provide critical constraints on megathrust slip for tsunami hazard assessments along the southern Cascadia margin. The theoretical fault sources of that (and this) study are probably not entirely accurate, because they do not

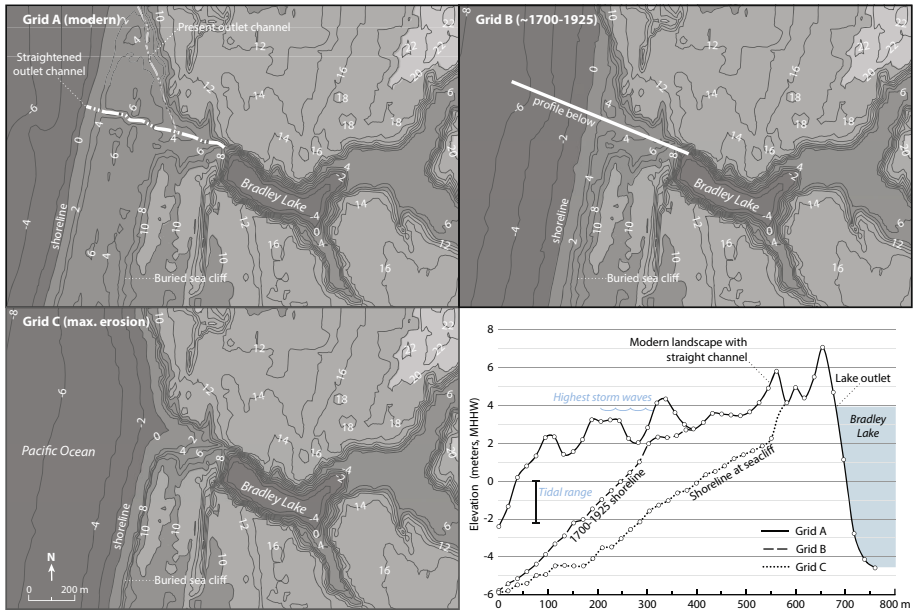


Fig. 3 Maps and profiles of numerical grids used in tsunami simulations referenced to the mean higher high water tidal datum (MHHW). Grid A reflects the modern topography derived from 2009 LiDAR data and includes a straightened outlet channel reconstructed from historical maps and photos (see Fig. 2). Grid B depicts the inferred landscape in AD 1700 based on the position of the shoreline in 1925 (Bernstein, 1925). Grid C represents the most landward possible position of the shoreline constrained by a paleosea cliff buried by sand dunes. Profiles (lower right) along the reconstructed outlet channel compare the modern topography (gray shade) to profiles from alternative model landscapes. Lake outlet elevation in all grids is ~ 4 m MHHW, equivalent to ~ 6 m (NAVD88). Grids A–C depict a progressive landward shift of the shoreline, respectively, thereby reducing barriers to tsunami inundation. Figure is modified from Witter et al. (2012)

account for viscoelastic effects and chaotic asperities; nevertheless, their models require 10–16 m of peak slip to simulate tsunami inundation in Bradley Lake. Since the barrier was breached 12 times in the past ~ 4600 years (Kelsey et al. 2005), any probabilistic or deterministic hazard analysis utilizing similar standard elastic fault models must input these minimum amounts of slip to account for the inundations.

Priest et al. (2014) simulated tsunamis for two southern Cascadia sources inferred from turbidite paleoseismology, “Segments C and D” (Fig. 1a) of Goldfinger et al. (2012). Rupture models for both sources entail symmetrically distributed slip on a buried megathrust fault. The simulations of tsunamis generated in southern Cascadia showed how rapidly wave heights decreased along strike to improve tsunami preparedness efforts in coastal communities in northern Oregon and southern Washington. Like thrust faults, which project greater seismic energy across strike than along strike (Shi and Brune 2005), deformation during subduction earthquakes generates tsunamis that direct the greatest energy perpendicular to the long axis of rupture (see Geist (1998) for summary). Tsunamis direct relatively less energy along strike, particularly for subduction zones like Cascadia where the rupture width is narrow relative to length.

In their analyses, Priest et al. (2014) hypothesized that tsunami deposits in Bradley Lake recorded tsunamis generated by Cascadia earthquakes that ruptured the megathrust directly offshore of the lake. Their models that used southern Cascadia ruptures placed most slip

Table 1 Cascadia earthquake scenario parameters that produce tsunami inundation in Bradley Lake modified from Witter et al. (2012) by changing all rupture lengths to the ~1100 km values used in the 2012 simulations and modifying magnitudes accordingly; simulations used a Manning coefficient of zero (zero friction); tsunami model = SELFE

Fault slip distribution	Length (km)	Width (km) ^a	Minimum peak slip deficit (years)	Max. peak slip 49°N (m)	Peak slip 43°N (m) ^b	Mean slip (m)	M_0 (10^{22} N m) ^c	Moment magnitude (M_w) ^d
<i>Modern topography, straight outlet channel (grid A)—MSL + 0.5</i>								
Symmetric slip	1100	105	500	20	16	10	4.5	9.0
Seaward-skewed slip ^e	1100	105	600	24	19	12	5.4	9.1
Splay fault slip	1100	83	460	18	15	9	3.3	8.9
<i>Circa 1925 shoreline (grid B)—MSL + 0.5</i>								
Symmetric slip	1100	105	400	16	13	8	3.6	9.0
Splay fault slip	1100	83	360	14	12	7	2.6	8.9
<i>Shoreline near seacliff (grid C)—MSL + 0.5</i>								
Symmetric slip	1100	105	290	11	9	6	2.6	8.9
Splay fault slip	1100	83	260	10	8	5	1.8	8.8
<i>Shoreline near seacliff (grid C)—MHHW</i>								
Symmetric slip	1100	105	270	11	9	5	2.4	8.9
Splay fault slip	1100	83	250	10	8	5	1.8	8.8

Tidal elevation used in simulations, Mean Sea Level (MSL) +0.5 m (1.55 m NAVD 88), approximates hindcast tide in AD 1700 (ref Mofjeld et al. 1997). Runs completed with grids A and B use MSL +0.5 m tide; runs completed with grid C use MSL +0.5 m and mean higher high water (MHHW, 2.07 m NAVD 88) tides

^a Equivalent width for entire fault; actual width at latitude of Bradley Lake is smaller

^b Slip estimates are the product of the recurrence interval times the convergence rate at latitude of Bradley Lake (32 mm yr⁻¹). Maximum slip estimates use a convergence rate close to 40 mm yr⁻¹

^c Seismic moment (M_0) = Fault area x slip x rigidity, where rigidity = 4×10^{10} N m⁻²

^d Moment magnitude (M_w) = (log M_0 -9.1)/1.5

^e The seaward-skewed slip rupture model was used only for tsunami simulations incorporating grid A

south of the lake and generated smaller tsunamis, less likely to inundate the lake. For example, tsunami simulations generated by rupture of segment D with 200 years of slip deficit release produced wave heights of only ~1.7 m offshore Bradley Lake (Priest et al., 2014; Fig. 4), which is too low to breach the ~6-m barrier into the lake. Furthermore, they noted that the 380- to 400-year average tsunami recurrence interval recorded at Bradley Lake (Kelsey et al. 2005) is similar to the average Cascadia earthquake recurrence interval inferred from turbidite paleoseismology north of the lake at Hydrate Ridge (320 years, Fig. 1a) but much longer than the turbidite recurrence interval south of the lake at Rogue Apron (segment D; 230 years, Fig. 1a). From this observation, Priest et al. (2014) reasoned that the turbidite record at Hydrate Ridge may provide a better estimate of Cascadia earthquake recurrence for tsunami hazard assessment in the vicinity of Bradley Lake. Our new experiments test their hypothesis and provide new constraints on megathrust slip during past Cascadia earthquakes.

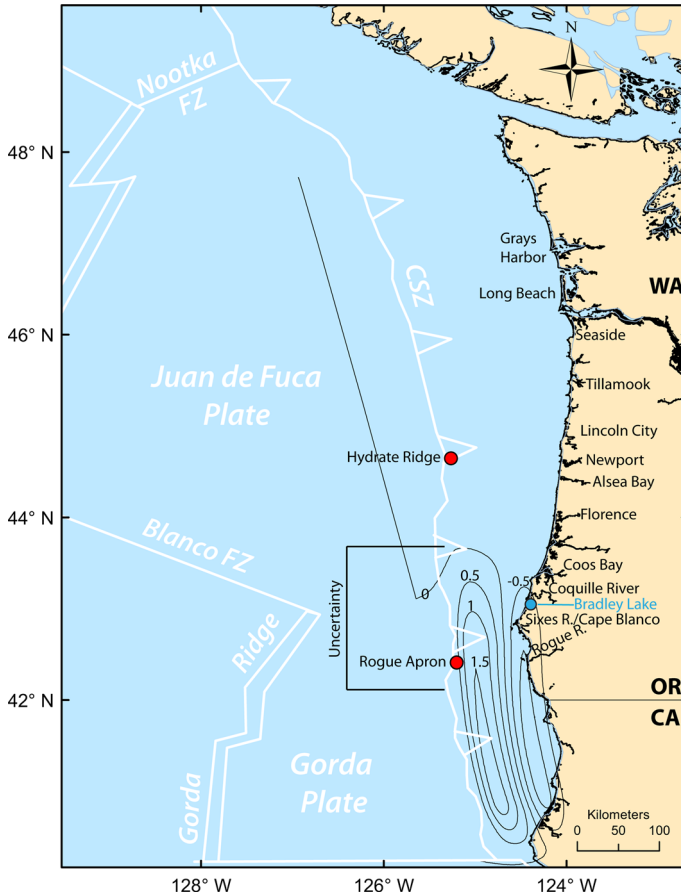


Fig. 4 Vertical coseismic deformation (0.5-m contours) of Priest et al. (2014) for a simulated southern Cascadia fault rupture releasing 200 years of slip deficit. Deformation from this source was linearly extrapolated to simulate sources for this study; positive numbers = uplift; negative numbers = subsidence. *Red dot* at Rogue Apron is location of core hole M9907-31PC-TC; red dot at Hydrate Ridge is core hole RR0207-56PC-TC; FZ Fracture Zone, CSZ Cascadia subduction zone, *seg.* segment, *Uncertainty* uncertainty in northern termination of southern Cascadia ruptures inferred from turbidites found in the Rogue Apron core hole but missing from the Hydrate Ridge core hole. R. River. Figure is modified from Priest et al. (2014)

3 Correlating marine and onshore records of Cascadia earthquakes and tsunamis

Correlations of paleoseismic records in Fig. 5 use data from studies of marine turbidites inferred to record strong shaking during great Cascadia subduction earthquakes in southern Cascadia (Goldfinger et al. 2012, 2013b, 2016a). We focus on two sites offshore Oregon: a structurally isolated slope basin west of Hydrate Ridge and a 2-km-wide apron at the base of Rogue Canyon ~250 km to the south (Fig. 1b). Turbidites at both sites include 10 rhythmic beds of sand and silt deposited along more than 580 km of the Cascadia margin from Rogue Apron in the South to Cascadia Channel in the north. These extensive “sandy turbidites,” identified in Fig. 5 as T1–T10 without lower case letters, have been interpreted

to record past great earthquakes caused by rupture along most of the length of the Cascadia subduction zone (Adams 1990; Goldfinger et al. 2012, 2013b, 2016a). Cores at Hydrate Ridge and Rogue Apron also contain dark intervals with silty bases that thicken sections of

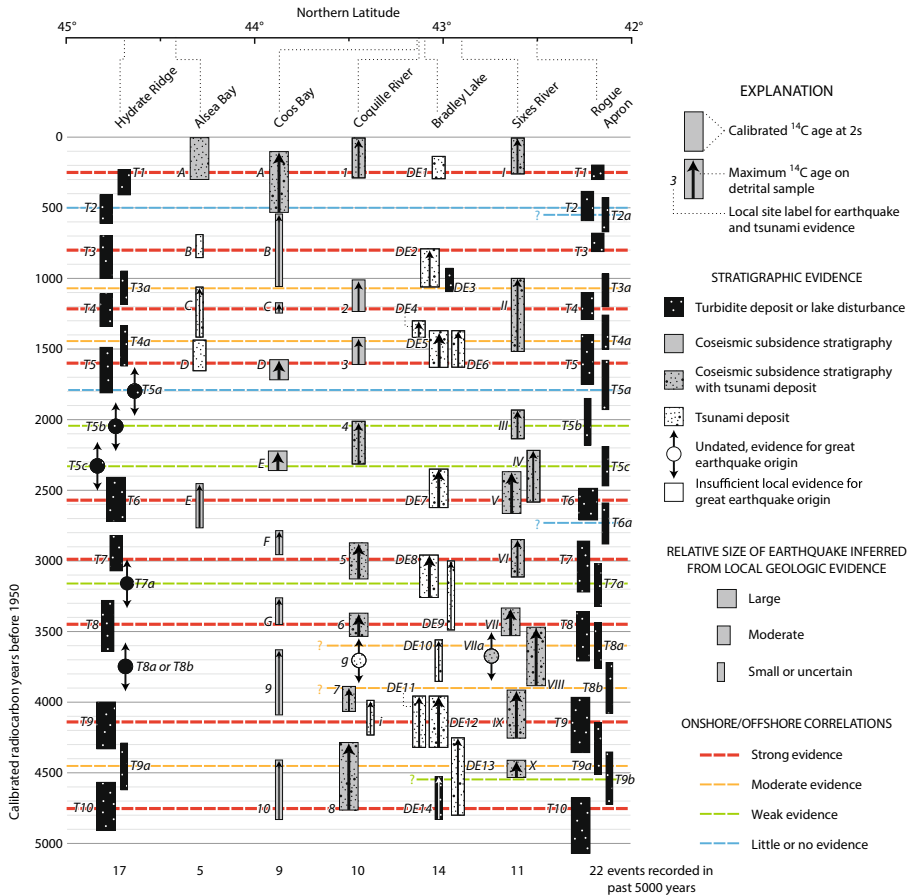


Fig. 5 Correlation of radiocarbon data from coastal paleoseismic sites in south-central Oregon and offshore turbidite sequences from Hydrate Ridge and Rogue Canyon (in Rogue Apron) modified from Witter et al. (2012) with additional data on Hydrate Ridge and Rogue from Goldfinger et al. (2013b, 2016a) and Coos Bay from Milker et al. (2016). Turbidites are labeled “T”; labels with “a”, “b”, or “c” are thin muddy turbidites; others are thicker sandy turbidites. Stratigraphic correlations of turbidites have been interpreted by Goldfinger et al. (2012) to reflect long (>500 km) fault ruptures (*bold dashes*) of most of the megathrust and shorter (<500 km) fault segment breaks (*thin dashes*) along the southern margin. *Up arrows* denote maximum age estimates on detrital samples. *Symbol width* represents relative size of earthquake inferred from deposit thickness or amount of subsidence evident in microfossil assemblages. *Rectangles* represent inferred earthquake age ranges in calendar years before 1950, calibrated from radiocarbon dates using Calib 5.0.2 software (Stuiver and Reimer 1993; M. Stuiver, P. J. Reimer, and R. W. Reimer, CALIB 5.0, 2005, available at <http://calib.qub.ac.uk/calib/>), the calibration database of Reimer et al. (2004) and the marine reservoir database of Hughen et al. (2004). The age ranges presented here have been recalibrated from the original laboratory reported age and are compiled in Goldfinger et al. (2012) or Goldfinger et al. (2013b). Original age data for Cascadia earthquake records from coastal sites are reported in studies at Alsea Bay (Nelson et al. 2008); Coos Bay (Nelson et al. 1996, 1998; Milker et al. 2016); Coquille River (Witter et al. 2003); Bradley Lake (Kelsey et al. 2005); and Sixes River (Kelsey et al. 2002). See Figs. 1b and 4 for geographic locations

pelagic clay deposited between sandy turbidites. These so-called muddy turbidites number 7 at Hydrate Ridge and 12 at Rogue Apron in the past 5000 years and are distinguished from sandy turbidites shown on Fig. 5 by lower case letters. Goldfinger et al. (2013b) attribute muddy turbidites in southern Cascadia to shaking during plate boundary earthquakes on the basis of their structure, distribution, and sedimentology.

We correlate the marine data with onshore geologic records of great subduction earthquakes and tsunamis in south-central Oregon at estuaries located between the latitudes of Hydrate Ridge and Rogue Apron. Evidence at estuaries comes from studies of Alsea Bay (Nelson et al. 2008), Coos Bay (Nelson et al. 1996, 1998; Milker et al. 2016), Coquille River (Witter et al. 2003), and Sixes River (Kelsey et al. 2002). Sharp contacts separating buried soils from overlying intertidal mud beneath estuary wetlands indicate episodes of sudden coseismic subsidence during great Cascadia earthquakes; widespread sand sheets that bury some soils at these estuaries evidence tsunamis generated by tectonic deformation offshore.

We also compare the history of marine turbidites to a record of Cascadia tsunamis revealed by distinctive and unusual disturbances in laminated lacustrine mud at Bradley Lake, a coastal lake located ~ 80 km north of Rogue Apron (Kelsey et al. 2005). Bradley Lake's proximity to the Pacific Ocean (~ 0.6 km) and the elevation of its outlet (~ 6 m above sea level) made it an optimal tsunami recorder over the past ~ 4600 years. A history of disturbances in the lake sediment during this period includes 12 landward-thinning sand sheets transported by sustained marine inundation, which Kelsey et al. (2005) attributed to large tsunamis generated by Cascadia earthquakes. They also found 2 layers composed of detrital terrestrial sediment deposited in the past 4600 years that interrupted the lake's typical laminated sediment, which probably mark times of seismic shaking that destabilized slopes along the lake margin. Kelsey et al. (2005) argued that the lake's 6-m-high outlet threshold prevented alternative marine processes from inundating the lake, like far-traveled tsunamis or extreme storms.

The comparisons of marine and onshore evidence for great earthquakes and tsunamis shown in Fig. 5 build upon correlations by Goldfinger et al. (2012) and Witter et al. (2012) that considered three aspects of the various datasets: (1) the stratigraphic model and sedimentary characteristics of marine turbidites at Hydrate Ridge and Rogue Apron; (2) the agreement (overlap) of 2-sigma calibrated radiocarbon age ranges; and (3) qualitative estimates of earthquake size, (e.g., turbidite mass, tsunami deposit thickness, or amount of subsidence). We rank possible correlations on the basis of strong, moderate, and weak evidence at different sites during a single event (Fig. 5). At Rogue Apron, 18 of 22 turbidites (81%) correlate with evidence onshore; and at Hydrate Ridge 15 of 17 turbidites (88%) correlate with evidence onshore. Correlations based on strong evidence (red dash, Fig. 5) include all sandy turbidites except T2, tsunami deposits in Bradley Lake and supporting evidence at many estuaries. Moderate evidence (orange dash, Fig. 5) supports correlations between muddy turbidites T3a, T4a, T8a, T8b, and T9a with tsunami deposits in Bradley Lake and additional evidence at estuaries. Weak evidence (green dash) suggests muddy turbidites T5b, T5c, T7a, and T9b may correlate with evidence at estuaries, but lack convincing evidence for tsunami inundation in Bradley Lake.

Four of the turbidites, observed at both Hydrate Ridge and Rogue Apron (T2, T5a, T5b, and T5c), imply a triggering rupture offshore Bradley Lake. However, these four turbidites, which suggest ruptures extending more than 550–800 km along the margin, have no correlative tsunami deposits at Bradley Lake, and sparse or equivocal evidence for correlative events at adjacent estuaries.

Another four turbidites observed only at Rogue Apron (T2a, T6a, T7a, and T9b) have been interpreted by Goldfinger et al. (2012, 2013b) to reflect ruptures of “Segment D” in the southern Cascadia subduction zone. Little or no evidence (blue dash, Fig. 5) supports correlation of these turbidites with tsunami deposits in Bradley Lake. Possible correlations of T7a with DE9 and T9b with DE13 require discounting alternative correlations based on greater evidence recorded in Bradley Lake, adjacent estuaries, and offshore turbidites.

Uncertainty in the 2-sigma age ranges which span several decades to hundreds of years, prevent conclusive correlations. For instance, many correlations have more than one possible alternative (e.g., T7a/DE9 versus T8/DE9). Furthermore, as Witter et al. (2012) point out, if any of the earthquake evidence includes multiple cascading ruptures that occurred within decades (e.g., Sieh et al. 2008), then they cannot be distinguished in these correlations. For additional description of radiocarbon age calibration methods and uncertainties, refer to Goldfinger et al. (2012).

4 Methods

4.1 Cascadia earthquake source

We simulate two CSZ rupture scenarios for three different purposes, a southern source to test for minimum slip to inundate Bradley Lake from the south and a full-margin source to test for continuity between our experiments and those of Witter et al. (2012) and for the effect of adding bottom friction to the tsunami simulations. The full-margin source extends nearly the full length of the CSZ and is identical to the symmetric buried rupture model of Witter et al. (2012; Fig. 2). The southern source is similar to the D200 model of Priest et al. (2014) (Fig. 4) with similar dimensions to ‘Segment D’ of Goldfinger et al. (2012). In both, all slip on both sources is assumed to be on the megathrust, thus there is no partitioning to a splay fault. Seismic reflection profiles south of latitude 42.8°N offer little evidence for a substantial splay fault (Goldfinger et al. 2016b).

Both sources taper slip to zero up and down dip on the megathrust from a peak value, resulting in a “bell-shaped” slip distribution centered roughly on the continental slope-shelf break. Peak uplift of the seafloor and overlying ocean occurs at the peak slip. Peak slip is calculated from the amount of time that plate convergence continues without release of slip in an earthquake (i.e., builds up slip deficit), assuming that the plates are completely locked. Coseismic slip for any value of slip deficit time therefore varies with latitude, depending on the local plate convergence rate. For this reason, we specify in experimental results the slip deficit time that it takes for the megathrust to build up enough peak slip to cause lake inundation.

We simulated coseismic vertical deformation in the same manner as Witter et al. (2012). The fault rupture model utilizes a realistic megathrust geometry and elastic coseismic deformation from the point source model of Okada (1985). A detailed description of the fault model is given in Witter et al. (2011, 2012, 2013) and Priest et al. (2014).

The southern CSZ rupture extends north from just north of Cape Mendocino at 40.4°N to near Cape Blanco at 42.75°N (Fig. 4) and has coseismic vertical deformation linearly scaled to simulate peak slip deficits differing from the 200 years utilized for the Priest et al. (2014) simulations. The north boundary of the southern CSZ rupture reflects the uncertainty in the northern limit of past ruptures that triggered turbidites in ‘Segment D’ proposed by Goldfinger et al. (2012). The uncertainty corresponds to a ~250-km gap in

marine core data between the Rogue Apron and Hydrate Ridge coring sites (Figs. 1b, 4) and by inferences of minimum turbidite triggering distances (Goldfinger et al. 2012; Black 2014). The slip and resulting vertical coseismic deformation of this source is tapered smoothly to zero between these limits of north–south positional uncertainty from ~Rogue River to ~Coos Bay (Fig. 4).

4.2 Tsunami simulation

Vertical components of surface deformation from the earthquake rupture are used to set up the initial water surface for tsunami simulations, assuming a short (10 s) initial constant acceleration of the seafloor and using a 1-s time step. Simulations of tsunami propagation and inundation use the hydrodynamic finite element model SCHISM derived from the model SELFE (semi-implicit Eulerian–Lagrangian finite element model) (Zhang and Baptista 2008; Zhang et al. 2011). SELFE was used by Witter et al. (2012) and is nearly identical to SCHISM software (Zhang et al. 2016b). Algorithms used to solve the Navier–Stokes equations in these models are computationally efficient and stable. SELFE passed all standard tsunami benchmark tests (Zhang and Baptista 2008; Zhang 2012) and closely reproduced observed inundation and flow depths of the 1964 Alaska tsunami in a trial at a site on the northern Oregon coast (Priest et al. 2010). SCHISM passed similar benchmark tests established by the National Oceanic and Atmospheric Administration (Zhang et al. 2016a).

The unstructured finite element mesh for each simulation is constructed by first compiling a digital elevation model (DEM) covering the project area and then retrieving from the DEM elevations at a series of points defining a triangular irregular network (TIN). The DEM for the regional simulations is compiled from the ETOPO1 1-arc-minute database (<http://www.ngdc.noaa.gov/mgg/global/global.html>) of the National Geophysical Data Center supplemented in areas of dry land by 2009 LiDAR data, and bathymetry of Bradley Lake from Kelsey et al. (2005). All data sets are adjusted to the North American Vertical Datum of 1988 (NAVD 88) (Zilkoski et al. 1992) and WGS 84 map projection. Computational grid spacing for tsunami simulations varies from ~3–5 km at the CSZ source to 4–5 m at the outlet channel of Bradley Lake. Each simulation is run long enough to record arrival of the peak tsunami wave at Bradley Lake.

Simulations use a Manning Coefficient of zero (zero bottom friction) as in the Witter et al. (2012) study. Although Titov and Synolakis (1997) note in their review that inundation results are not particularly sensitive to changes in bottom friction, one simulation uses a standard Manning Coefficient of 0.025 to assess the effect of including friction.

4.3 Variations in coastal landscape

Since the early 1900s, Oregon’s coastal dunes have been modified by the introduction of exotic plants (e.g., European beach grass, *Ammophila arenaria*) aimed at stabilization of sand dunes, creating a modern landscape not encountered by prehistoric tsunamis. We used the landscapes of Witter et al. (2012) to examine how late Holocene and historical landscape changes may have influenced tsunami inundation. The simulations used three different unstructured grids depicting hypothetical shorelines that vary in proximity to the lake (grids A, B, and C, Fig. 3). These paleolandscapes are based in part on observations of 1939 aerial photography and coastal survey maps from circa 1925 that portray the lake’s outlet channel as straighter and more easily flooded by tsunamis than its present outlet (see grid A, Fig. 3). Grid A depicts the straightened outlet channel on modern topography

derived from LiDAR collected in 2009 (Fig. 3). Grid B removes foredunes accentuated by vegetation planted in the 1930s (Komar 1997) and shifts the shoreline ~250 m east to near its position in the 1920s (Fig. 3). Grid B reflects the best estimate of Witter et al. (2012) of likely conditions in AD1700 and probably for the earlier shorelines after they aggraded seaward following coseismic subsidence events. Grid C depicts the shoreline in its most landward position interpreted from the geomorphic expression of a sea cliff buried by Holocene dune sand and located ~300 m east of the modern shoreline in grid A (Fig. 3). Grid C probably simulates erosion after a large coseismic subsidence event. Grids B and C are thus most representative of the range of paleolandscapes present prior to contemporary changes in the landscape caused by the introduction of European beach grass.

Other variations in coastal landscape are possible but are probably less important than variations in shoreline erosion and are beyond the scope of the project. For example, variations in the sinuosity of the outlet channel or deflections of the channel north or south are not simulated. Modest increases in tsunami travel distances over the straight channels in grids A, B, and C caused by these variations are probably less important controls of inundation than increases in shoreline water depth when erosion creates steeper beach profiles and shorter travel distances. It is also possible that the buried sea cliffs marking the position of the grid C shoreline represent a pre-Holocene landscape, but they are still useful because Holocene erosion could not have advanced any further.

4.4 Variations in ocean level relative to lake level

Diurnal fluctuations in sea level probably influenced whether tsunamis reached Bradley Lake (Kelsey et al. 2005). As in the Witter et al. (2012) investigation, simulations are run at two tide levels, one for the hindcast tide during the AD1700 tsunami and one at mean higher high water (MHHW). The tide in AD1700 is 1.55 m relative to the NAVD 1988 vertical datum. MHHW is 2.07 m NAVD88 based on the Port Orford, Oregon tide gauge in southern Oregon. Tsunami simulations at MHHW on the most landward shoreline, grid C, examined conditions most favorable for tsunami inundation of the lake. Simulations at the lower tide and the more seaward shoreline present in AD1700 (grid B) test for less favorable conditions for inundation most likely to have been present in the late Holocene.

Relative sea level also fluctuated when inter-seismic strain caused coastal uplift and earthquakes caused rapid subsidence. Witter et al. (2012) argued that inter-seismic relative sea level change could be ignored for the AD1700 landscape owing to slow vertical strain between earthquakes and late Holocene eustatic sea level rise because such small variations, <0.3 m since AD1700 (Witter et al. 2003), fall within the uncertainty of climate-related processes controlling ocean levels (e.g., ENSO; Komar et al. 2011). Sea level relative to the lake outlet elevation for earlier times is uncertain, because it would likely be dependent on fluctuations in the prevailing water table and influx of mobile sand dunes.

5 Results

Tsunami simulations that inundate the lake require higher coseismic slip for model landscapes with lower sea levels and more seaward shorelines regardless of the CSZ source used (Fig. 3; Segment D values in Table 2). Using the estimated sea level at the time of the AD1700 event (1.55 m (NAVD88)), simulations with the most seaward shoreline, grid A, require the release of at least 850 years peak slip deficit for inundation. Simulations that

Table 2 Cascadia earthquake scenario parameters of this investigation that produce tsunami inundation in Bradley Lake; n = Manning coefficient (friction) See Fig. 1a for explanation of Cascadia subduction zone (CSZ) segments A and D

Fault slip distribution (csz segment)	Length (km)	Width (km) ^a	Minimum peak slip deficit (years)	Tsunami model	n	Max peak slip (m)	peak slip at lake (m) ^b	mean slip (m)	M_0 (10 ²² N m) ^c	Moment magnitude (M_w) ^d
<i>Modern topography, straight outlet channel (grid A) —MSL + 0.5</i>										
Symmetric slip, (segment D)	364	61	850	SCHISM	0.000	29	16	14	1.3	8.7
<i>Circa 1925 shoreline (grid B) —MSL + 0.5</i>										
Symmetric slip, (segment D)	364	61	640	SCHISM	0.000	22	12	11	0.9	8.6
<i>Shoreline near seacliff (grid C)—MSL + 0.5</i>										
Symmetric slip, (segment A)	1100	105	290	SCHISM	0.000	11	9	6	2.6	8.9
Symmetric slip, (segment A)	1100	105	290 ^e	SELF	0.000	11	9	6	2.6	8.9
Symmetric slip, (segment A)	1100	105	290	SCHISM	0.025	11	9	6	2.6	8.9
Symmetric slip, (segment D)	364	61	500	SCHISM	0.000	17	9	8	0.7	8.5
<i>Shoreline near seacliff (grid C)—MHHW</i>										
Symmetric slip, (segment D)	364	61	430	SCHISM	0.000	15	8	7	0.6	8.5

Tidal elevation used in simulations; mean sea level (MSL) +0.5 m (1.55 m NAVD 88), approximates hindcast tide in AD1700 (ref Mofjeld et al. 1997). Runs completed with grids A and B use MSL +0.5 m tide; runs completed with grid C use MSL +0.5 m and mean higher high water (MHHW, 2.07 m NAVD 88) tides
^a Equivalent mean width for entire fault; actual width at latitude of Bradley Lake is smaller for the 1100-km rupture length, approximating the 61 km listed for the 364 km length

^b Slip estimates are the product of the recurrence interval times the convergence rate at latitude of Bradley Lake (32 mm yr⁻¹) for the 1100-km rupture and mean rate at the Gorda Plate of 34 mm yr⁻¹ for the Segment D source; modeled slip at Bradley Lake for Segment D is based on the assumption that slip tapers linearly over the range of uncertainty in the northern termination of the rupture (Fig. 4) from turbidite data of Goldfinger et al. (2012). Maximum peak slip estimates use a convergence rate close to 40 mm yr⁻¹ for full-margin ruptures and 34 mm yr⁻¹ for Segment D ruptures

^c Seismic moment (M_0) = Fault area x slip x rigidity, where rigidity = 4×10^{10} N m⁻²

^d Moment magnitude (M_w) = $(\log M_0 - 9.1)/1.5$

^e Results from Witter et al. (2012) using the SELF

inundate the lake using grid B, the AD1700 landscape with a shoreline between grids A and C, require minimum of 640 years peak slip deficit release. A minimum of 500 years peak slip deficit release is required for grid C, the most landward shoreline. The minimum slip deficits for simulations on grids B and C provide the most reasonable constraints, because both remove dune accretion from modern introduction of European beach grass. When sea level is increased to MHHW (2.07 m (NAVD88)), simulations require a minimum of 430 years of peak slip deficit release to inundate the lake on grid C (Table 2). Obviously all of these slip deficits are minima to breach the lake outlet, so larger values are possible.

The lake outlet in all of the southern Cascadia simulations is first breached by tsunami waves emanating from the coseismic deformation directly offshore rather than by refracted waves or the edge waves that travel north from the much larger coseismic deformation to the south (Fig. 4). Representative snapshots of five animations at the point of initial lake inundation illustrate that inundation occurs between 20.5 and 22.5 min for the Segment D source (Fig. 6a–d), similar to the 24.7 min for the full margin, Segment A source (Fig. 6e). Representative time histories from simulations of Witter et al. (2011) and Priest et al. (2014) illustrate that these inundation times are from peak waves starting from coseismic deformation directly offshore (Fig. 6f). Note that later edge waves and refracted waves from the main coseismic deformation of the Segment D source south of Cape Blanco (Fig. 4) are approximately half or less of the peak wave height (Fig. 6f). It is clear that had we simulated inundation from a source terminating slip some distance south of the lake, approximately twice as much slip would have been required to inundate the lake on the three grids.

Changing the tsunami software from SCHISM to SELFE and altering assumed bottom friction (Manning coefficient) from zero to the standard value of 0.025 did not alter results. All of the simulations testing these factors on Grid C with tide at 1.55 m (NAVD88) required a minimum of 290 years of slip deficit to cause tsunamis to inundate the lake (Segment A results in Table 2).

6 Discussion

Our new simulations demonstrate that southern Cascadia ruptures with slip concentrated south of Bradley Lake are unlikely to produce tsunamis surmounting the lake outlet, especially if slip terminates south of the lake. For example, Witter et al. (2003), Kelsey et al. (2005), Burgette et al. (2009), and Goldfinger et al. (2012) all made geological arguments for the Cape Blanco area being a potential barrier to propagation of slip from southern Cascadia ruptures. The simulations account for slip deficits available from inter-event plate motion and show inefficient along-strike projection of tsunami energy in the form of edge and refracted waves from the south. These findings led us to reassess coseismic slip estimates consistent with tsunami inundation by using turbidite inter-event times for the turbidite record at Hydrate Ridge (core RR0207-56PC-TC) from Goldfinger et al. (2012, 2013b), which record CSZ ruptures with megathrust slip directly offshore of Bradley Lake (i.e., ruptures that continue north of Segment D of Goldfinger et al. 2016a, Fig. 1a).

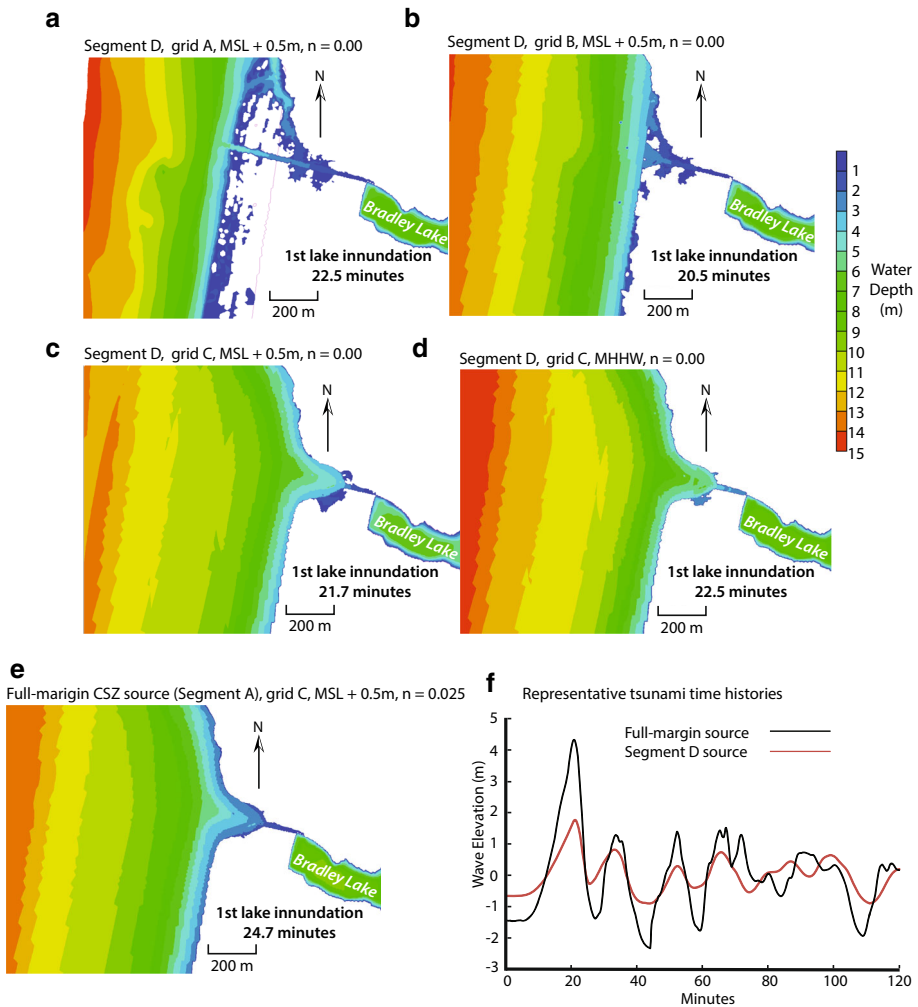


Fig. 6 a–e Snapshots of representative animations of inundation showing the time after a CSZ earthquake that the tsunami first inundates Bradley Lake. **f** representative tsunami time histories near the Bandon shoreline 6 km north of Bradley Lake; the Segment D source is the same as in 6a–6d but with slip deficit release reduced to 200 years (data from scenario D200 of Priest et al. 2014); full-margin CSZ source is the same as in 6e but with slip deficit release increased from 290 to 300 years (data from scenario Sm2 of Witter et al. 2011). *MSL* mean sea level, *n* Manning coefficient

6.1 Improved constraints on megathrust slip

Our simulations of a southern Cascadia source (Fig. 4) demonstrate that earthquakes capable of producing tsunamis that inundate Bradley Lake from this source must have coseismic slips that approach the upper limits expected from global data for a slip patch that is only ~ 300 km long and ~ 60 km wide. Minimum peak slip deficit of 430–640 years (15–22 m peak slip for grids C and B, respectively) from M_w 8.5–8.6 earthquakes (Table 2) is needed to produce lake inundation for the most likely late Holocene landscapes. These magnitudes fall between empirical estimates for rupture

patches this size based on linear regressions through modern seismic data of Blaser et al. (2010). Using their preferred oceanic thrust (subduction zone) data, the inferred M_w from the 60-km rupture width or ~ 300 -km length would be 7.9 or 8.7, respectively, thus total moment values could conceivably fit within those global data. However, mean slips for these simulations are higher than would be expected from global data for subduction zone ruptures 300 km long, except for the most landward shoreline (grid C). For example, the Scholz (1982) ratio of mean slip to length of 2×10^{-5} predicts mean slip of 7 m, similar to the minima of 7–8 m for inundation of the lake on grid C, but much smaller than 11 m required of the other likely landscape (Table 2). Likewise, seismic energy balance calculations of Scholz (2014) predict an average of only 6.8 m slip for Segment D ruptures of Goldfinger et al. (2012) and a sum of seismic moments for all Holocene Segment D events, equaling only 3% of the total available from plate convergence.

These values of 7–11 m are also minima for two reasons: (1) Modeled sea level relative to the lake outlet barrier is significantly higher than prior to ~ 1000 years ago, and (2) some southern CSZ ruptures probably stopped in the vicinity of Cape Blanco (e.g., Witter et al. 2003; Kelsey et al. 2005; Burgette et al. 2009; Goldfinger et al. 2012). Southern Cascadia ruptures that terminate at Cape Blanco would not deform the seafloor directly offshore Bradley Lake (Fig. 4), which is the primary mechanism responsible for the peak wave height (Fig. 6f). The consequent reduction in wave height (and increase in needed slip to inundate the lake) could be as much as a factor of two based on the height of edge waves and refracted waves relative to the peak wave (Segment D source, Fig. 6f).

From our analyses, it appears that southern CSZ ruptures (Fig. 1a) release too little slip deficit north of Cape Blanco (Fig. 4) to produce tsunamis large enough to reach Bradley Lake. If some southern CSZ ruptures produced tsunamis large enough to inundate the lake, then the ruptures may have had unusually large slip relative to their length and occurred during higher tides or washed over landward shorelines that promoted tsunami inundation. One of the turbidites, T8a or T8b (that correlate to tsunami deposits DE10 and DE11, respectively), may record such a southern CSZ earthquake (Fig. 5; Table 3). Even this rupture could have extended north of Cape Blanco, as there is not enough spatial resolution of the paleoseismic records onshore or offshore to constrain the event by event history at this suspected segment boundary (i.e., see marine core sites in Fig. 1a).

If southern Cascadia segment ruptures mostly ending or decreasing slip near Cape Blanco are unlikely sources for lake-inundating tsunamis, then longer ruptures that include slip offshore Bradley Lake are more likely to generate the lake-inundating tsunamis. This hypothesis leads to an alternative analysis of constraints by tsunami simulations on slip balance from that of Witter et al. (2012), which included all Segment D events recorded in turbidite data at Rogue Apron (and sites further south). The best and closest record of CSZ ruptures that likely extended north of the Segment D boundary is the turbidite data at Hydrate Ridge from Goldfinger et al. (2012, 2013b; Fig. 4; Table 3). The Hydrate Ridge record has 32 events over the last ~ 9650 years (Goldfinger et al. 2013b, 2016a), yielding an average return period of ~ 310 years. The Witter et al. (2012) minimum peak slip deficits of 8–13 m for lake inundation on the most likely landscapes, grid B and C (Table 1) require 270–400 years of strain accumulation at full plate locking. Thus the Hydrate Ridge average recurrence time is bracketed by a range of slip models capable of depositing tsunami sands in Bradley Lake. Over the past 4600 years, the range of interest for Bradley Lake, there were 17 turbidites at Hydrate Ridge, yielding an average repeat time of 270 years, or just at the lower end of the slip deficit release required to generate Bradley Lake tsunami deposits, assuming time is a good indicator of strain accumulation and release per event. During the same period, Bradley Lake preserved 12 tsunami deposits

Table 3 Correlation of Bradley Lake tsunami deposits and lake disturbances to the turbidite record

Bradley Lake disturbance event	Inferred tsunami size (Figure 5)	Bradley Lake Recalibrated ages ^a	Bradley Lake median age ^a	Marine turbidite number ^a	Marine turbidite inferred mean age ^a	Rogue Apron turbidite age ^b	HydrateRidge turbidite age ^b	Northernmost Segment Ruptured ^d
DE1	Large	280–310	300	T1	270	200–300	230–410	A
				T2	480	380–590	410–610	A
				T2a	550	430–670		D
DE2	Large	790–1070	950	T3	800	680–810	700–1000	A
DE3	Small	920–1170	1010	T3a	1070	970–1200	950–1180	C
DE4	Medium	1300–1480	1370	T4	1240	1100–1290	1110–1340	A
DE5	Large	1340–1700	1500	T4a	1420	1260–1500	1330–1620	C
DE6	Medium	1340–1700	1500	T5	1550	1420–1750	1490–1810	A
				T5a	1820	1580–1930	no date	C
				T5b	2040	1850–2180	no date	B?
DE7	Large	2350–2620	2510	T6	2540	2490–2710	2410–2720	A
				T6a	2730	2590–2880		D
				T7	3030	2860–3220	2820–3070	A
DE8	Large	3000–3250	3130	T7a ^c	3160	3020–3320	no date	C ^e
				T8	3440	3360–3710	3280–3640	A
DE10	Small	3630–3840	3730	T8a	3600	3440–3760	no date ^e	D or C ^e
DE11	Medium	4080–4350	4200	T8b	3890	3720–4080	no date ^e	D or C ^e
DE12	Large	4080–4410	4210	T9	4110	3780–4130	4000–4330	A
DE13	Medium	4240–4570	4430	T9a	4440	4140–4510	4290–4620	C [?]
				T9b	4610	4360–4730		D
DE14	Small	4570–4840	4700	T10	4770	4680–5070	4570–4910	A

Colors indicate degree of correlation by Goldfinger et al. (2012) as follows: Good age match = < ~100 years (green); fair match = 100–150 years (blue); poor match = 150–200 years (gray)

Recalib recalibrated, *Disturb.* disturbance of lake sediments probably by an earthquake, *mod.* moderate

^a Data are from Goldfinger et al. (2012)

^b Data encompass $\pm 2\sigma$ error for turbidite ages from cores M9907-31PC-TC (Rogue Apron) and Core RR0207-56PC-TC (Hydrate Ridge) from Goldfinger et al. (2013b)

^c Mean age is from Rogue Apron data where there is no data at Hydrate Ridge or where range at Hydrate Ridge exceeds Rogue Apron range by >50 years

^d Segment assignments are from Goldfinger et al. (2016a) based on northernmost extent of each turbidite. Note that Goldfinger et al. (2016a) rupture lengths and labels differ from Goldfinger et al. (2012), except for Segment D. For example, Segment C[?] of Goldfinger et al. (2016a) approximates Segment C of Goldfinger et al. (2012); Segment C of Goldfinger et al. (2016a) extends north of the Segment C of Goldfinger et al. (2012)

^e Goldfinger et al. (2012) found one turbidite layer in the Hydrate Ridge core that could correlate to either T8a or T8b in the Rogue Apron core, but there was no data for this layer that could resolve which might correlate

(Kelsey et al. 2005) with a return period of 380 years (Fig. 5; Table 3). We suggest that this alternative analysis is an acceptable and improved alternative view of the sources and timings of potential sources for the Bradley Lake tsunami record. This evaluation of the earthquake time series considering turbidite recurrence times at Rogue Apron compared to Hydrate Ridge has implications for slip budgets on the CSZ.

6.2 Hypothetical megathrust slip budgets

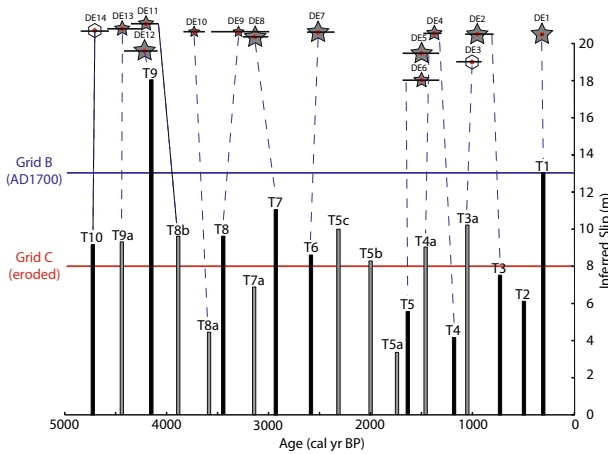
We devised hypothetical megathrust slip budgets to assess whether or not the total available slip deficit and slip deficit times between earthquakes from the Hydrate Ridge data are consistent with minimum slip to cause the 12 lake inundations in the last ~4,600 years. To construct hypothetical slip budgets and slip deficit histories for the Hydrate Ridge and Bradley Lake paleoseismic records (Fig. 7), we assume that slip available for fault rupture patches near Bradley Lake has accumulated in the past 4700 years (since the deposition of turbidite T10, Table 3) at the local convergence rate of ~32 mm/yr (Wang et al. 2003) (slope of the dashed line in Fig. 7c). We also assume a coupling coefficient of 1.0 (Scholz and Campos 2012; McCaffrey et al. 2013; Scholz 2014) so convergence time equals peak slip deficit time.

We test two models proposed by Shimazaki and Nakata (1980) for release of the slip deficits in subduction zone earthquakes: a time-predictable model where the time between two earthquakes is proportional to coseismic slip of the preceding earthquake (i.e., follow time = slip) and a slip-predictable model where the slip deficit built up before an earthquake equals its slip (i.e., preceding time = slip). Figure 7a shows a slip history based on turbidite follow times and Fig. 7b the slip history for preceding times. Because we do not know whether turbidite deposits T8a or T8b extend to Hydrate Ridge from Rogue Apron, but do know that both may correlate to Bradley Lake tsunami deposits (Goldfinger et al. 2012), we include both in the analysis.

Results clearly show that turbidite inter-event times are at best modest predictors of coseismic slip. The best known event is the AD1700 tsunami and earthquake that had ~19 m slip estimated by Satake et al. (2003). Wang et al. (2013) estimated 17.6 m (550 years slip deficit) near the latitude of Bradley Lake from paleocoseismic subsidence, while Witter et al. (2012) estimated 12–13 m minimum slip (360–400 years slip deficit; Table 1) to account for inundation of the lake. The ~250 years between T1 and T2 (7.8 m slip deficit) would suggest that the T1 tsunami would not have inundated the lake, if the preceding time was indicative of coseismic slip (Fig. 7b). The follow time for T1 is unknown, being >316 years (10 m slip), so the follow time fits that event better as concluded independently by Goldfinger et al. (2012). T2 did not produce a tsunami deposit in the lake, which is consistent with the 7.8 m slip predicted by its follow time.

For events before T2 neither the follow times nor preceding times correspond very well with the 8-m minimum peak slip required to cause lake inundation. For example, both cases predict lake inundation for T5c and T5b, but there are no corresponding tsunami deposits or seismic disturbances in the lake sediment obvious enough to be identified in the analysis of Kelsey et al. (2005) (Table 3; Fig. 7a, b). Similarly, both cases predict no inundation for T5, although the lake was apparently inundated by a moderate tsunami during this event (Fig. 7a, b). Goldfinger et al. (2012) analyzed the Holocene time series for goodness of fit to both time and slip-predictable models, with coefficients of 0.31 and 0.06, respectively, and noted that the time-predictable model provides a moderately better fit than the slip-predictable model.

a Slip from turbidite following time interval



Explanation a & b

T5 Sandy turbidite, height = slip based on inter-turbidite time and convergence at 32mm/yr; Goldfinger et al. (2012) labels

T5a Hydrate Ridge muddy turbidite, height = slip based on inter-turbidite time and convergence at 32mm/yr; Goldfinger et al. (2012) labels

DE12 DE11 DE10
Large, medium, small tsunami deposit in Bradley Lake with 2 sigma error on age; Kelsey et al. (2005) labels

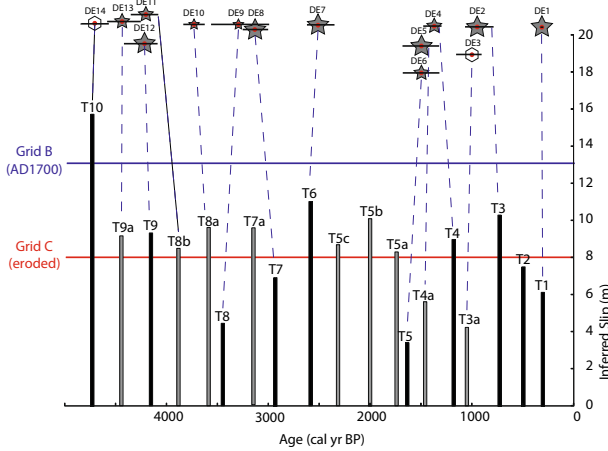
DE14
Disturbance event in Bradley Lake with 2 sigma error on age; Kelsey et al. (2005) labels

— Correlation of turbidite to Bradley Lake disturbance or tsunami deposit by Goldfinger et al. (2012)

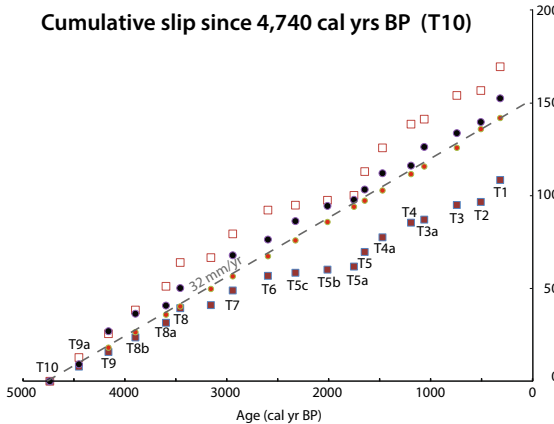
— Minimum slip for lake inundation from ruptures directly offshore (most likely seaward shoreline, grid B)

— Minimum slip for lake inundation from ruptures directly offshore (most landward shoreline, grid C)

b Slip from turbidite preceding time interval



c Cumulative slip since 4,740 cal yrs BP (T10)



Explanation c

□ Case 1: high min. slip for tsunamis in lake = 13 m; min. slip for earthquake with no tsunamis in lake = 2.7 m

■ Case 2: low min. slip for tsunamis in lake = 12 m; min. slip for earthquake with no tsunamis in lake = 1.7 m

• Case 3: slip = turbidite following time interval times 0.032 m/yr convergence rate

• Case 4: Slip = turbidite preceding time interval times 0.032 m/yr convergence rate

◀ **Fig. 7** Subduction zone fault slip and slip balance over the last ~4700 years (since turbidite T10) from turbidite record at Hydrate Ridge plus one turbidite (T8a or T8b) at Rogue Apron. **a** Coseismic slip inferred from turbidite following time (set at 13 m for the last event at T1 based on our simulation); **b** Coseismic slip inferred from turbidite preceding time; **c** Cumulative slip since turbidite T10 for four cases: Case 1, slip = high minimum to get tsunamis into Bradley Lake of 13 m and, for turbidites T2, T5a, T5b, and T5c without matching tsunami deposits in the lake, the high minimum of 2.7 m to produce a turbidite; Case 2, slip = low minimum to get tsunamis into Bradley Lake of 12 m and, for turbidites T2, T5a, T5b, and T5c without matching tsunami deposits in the lake, the low minimum of 1.7 m to produce a turbidite (*filled squares*); Case 3, turbidite follow times; Case 4, turbidite preceding times. Data are from Goldfinger et al. (2012, 2013b). Min. = minimum. Note that total slip must approximately balance with total plate convergence for either Case 3 or Case 4, since they both use inter-event age data

The inter-event times for the Hydrate Ridge turbidites do, however, predict slip values more consistent with Bradley Lake tsunami inundations than inter-event times at Rogue Apron. Witter et al. (2012) found that only 4 of the last 12 inundations of the lake are consistent with the Rogue Apron turbidite record. Using mainly the Hydrate Ridge data, follow times are consistent with 8 of the 12 inundations (Fig. 7a) and preceding times with 7 of the 12 (Fig. 7b). Therefore, we concur with the conclusion of Witter et al. (2012) that times between turbidites are not reliable predictors of slip, probably reflecting slip deficit accumulated over multiple earthquake cycles before being released (See also Goldfinger et al. 2013a). However, eliminating most Segment D turbidites from such analyses doubles the number of events that predict tsunami inundation. This improved fit does not provide a positive link between the onshore and offshore; however, it demonstrates that using the most appropriate paleoseismic data is required before conclusions regarding fit or misfit of various disparate records can be drawn.

We also examine whether the ~150 m of slip deficit available from plate convergence in the last ~4700 years can produce both the tsunamis that inundated Bradley Lake and the minimum shaking to trigger the turbidites at Hydrate Ridge. In Fig. 7c we illustrate cumulative slip from the turbidite following (Case 3) and preceding times (Case 4), where slip is forced to approximate the available ~150 m, compared to two cases for minimum slips which account for CSZ earthquakes with and without inundations of the lake: Case 1) a high minimum of 13 m slip to get tsunamis into Bradley Lake on the most seaward likely shoreline (AD1700 landscape, grid B) combined with a high minimum of 2.7 m slip to produce a turbidite for earthquakes without tsunami evidence in the lake; and Case 2) a low minimum of 8 m slip to inundate the lake for the most landward, eroded shoreline (grid C) for events before AD1700 combined with a low minimum of 1.7 m slip to produce a turbidite for CSZ earthquakes without tsunami inundation of the lake. The minimum peak slips of 1.7 and 2.7 m are inferred from the threshold of M_w 7.0–7.4 to produce a turbidite (Goldfinger et al. 2013b) by estimating peak slip from magnitude using empirical data of Rodríguez-Pérez and Ottemöller (2013) for subduction zone events with M_w between ~6.5 and 8.0. It is apparent from Fig. 7c that using the high minimum slips (Case 1) overshoots available slip by ~25 m while using the low minimum slips (Case 2) falls short by ~40 m. Of course, many possibilities exist between Cases 1 and 2, but the two illustrate that it is possible for the CSZ to produce both the turbidite and paleotsunami records, if Segment D events are not considered.

Since either T8a or T8b at Rogue may represent ruptures terminating south of Hydrate Ridge and potentially south of Bradley Lake, counting both of them in the slip balance at the latitude of the lake or Hydrate Ridge is problematic. In Cases 1 and 2, we assign peak slips of 13 and 8 m, respectively, to T8a and T8b. If instead we assume that either T8a or T8b, released the minimum 22 m slip (most likely seaward shoreline, grid B) or 15 m

(most landward shoreline, grid C) to inundate the lake from the modeled southern CSZ source (Fig. 4), then we can delete 13 m (Case 1) to 8 m slip (Case 2) for one event from the slip budget. The overshoot for Case 1 would then decrease to ~ 12 – 17 m and undershoot for Case 2 would increase to ~ 48 – 53 m. Thus for the 17 earthquakes that produced turbidites at Hydrate Ridge in the last ~ 4700 years, there is a maximum of 48 – 53 m (~ 3 m per event) to accommodate those with slip between the turbidite and lake inundation thresholds or more than the threshold for inundation.

Witter et al. (2012) did a similar analysis of slip balance including all 23 turbidites at Rogue Apron. They came to conclusions similar to ours, finding that there is little slip available for the 11 turbidites that lack correlative deposits in Bradley Lake if each deposit corresponds to the high minimum of 12 – 13 m. They noted that only 57 m of slip is available for these 11 events (a mean of ~ 5.2 m of slip per event) assuming the minimum of 8 m for the events that inundate the lake on the most landward shoreline (grid C).

The relatively small amount of slip deficit available from plate convergence to account for more than minimal slip to trigger turbidites and lake inundation has several possible explanations, including: (1) lack of correspondence between the theoretical fault dislocation model and actual coseismic deformation, (2) inherent uncertainties in turbidite data for specification of CSZ rupture lengths or recurrence, and (3) limitations of the tsunami model in simulating all energy imparted to the water column during coseismic rupture. For example, we do not include energy imparted to the ocean by the lateral component of fault motion, only the vertical, and simulate the vertical component of seafloor acceleration during rupture by simply raising the seafloor in 10 1-s steps. The horizontal component of fault motion can be significant for tsunami generation (e.g., Nicolosky et al. 2013), although the effect may not be as important for our simulations of CSZ sources owing to the assumption of decreasing coseismic slip across the continental slope where horizontal displacement effects would be most pronounced (i.e., our assumption of velocity strengthening behavior in the outer part of the megathrust).

Any of the preceding issues might explain the offshore Bradley Lake mismatch. However, more fundamentally, CSZ strain stored need not correspond well or at all to the inter-event times over the long term. If the CSZ relieves accumulated strain during long term “super cycles” as inferred by Goldfinger et al. (2013a), the overall coseismic release will track plate motion as before, but individual cycles may not, and may release more or less strain energy than expected in any single event. In this case, inter-event following times and preceding times plotted in Fig. 7a and b need not fit either the time- or slip-predictable models, respectively, of Shimazaki and Nakata (1980).

Considering the supercycle model and the potential for long-term memory of previous cycles, the long ~ 1000 -year gap in margin-wide ruptures that followed T6 may relate to the series of short interval moderate earthquakes that preceded T6, and could have reduced the overall energy storage level of the CSZ to a low value (See Goldfinger et al. 2013a, their Fig. 4). The lack of inundations or earthquake-induced disturbances of sediment in Bradley Lake by the T5a, T5b, and T5c earthquakes may have been caused by their occurrence during a time of elastic energy storage on the megathrust, and the intervening T5a, T5b, and T5c events may have been smaller than expected from plate motion alone. In addition, inter-seismic uplift would be larger than average during much of that period, raising the lake outlet relative to MSL.

Do the minimum slips for lake inundation approximate what would be expected from seismic energy balance considerations over the last 10,000 years of the paleoseismic record? Scholz (2014) concluded that stress drop is approximately constant in Cascadia earthquakes, and, because stress drop is proportional to slip divided by rupture width, slip

is proportional to width. It follows that slip must decrease from north to south in each CSZ earthquake since the width of the likely coseismic ruptures decreases to the south (Fig. 1). He argued that the width of full seismic coupling decreases from ~ 100 km in northern Cascadia to ~ 40 km near Bradley Lake and south. He then calculated the average amount of slip that should be released in order to achieve slip balance in each part of the CSZ while still honoring the number of earthquakes and rupture lengths inferred by Goldfinger et al. (2012) from turbidite data. He calculated a value of ~ 10 m at the latitude of Hydrate Ridge and ~ 8 – 7 m from Bradley Lake south. The ~ 10 m slip estimate is probably more appropriate for Bradley Lake since it is derived by excluding Segment D ruptures, that, as mentioned previously, may terminate or decrease in slip north of Cape Blanco. In any case, these values overlap the minimums to cause lake inundation, consistent with the observation that most of the earthquakes recorded as turbidites at Hydrate Ridge appear to correlate with inundations (Table 3, Figs. 5, 7a).

6.3 Effect on estimate of slip for sea levels lower than simulated

The paleolandscapes tested here and by Witter et al. (2012) reflect sea levels close to modern levels that prevailed since about 1000 years ago, so slip deficits larger than the 250- to 600-year minimums would be needed to produce tsunamis that could breach the lake outlet in earlier times when sea level was lower; up to 4 m lower at 4600 years B.P (e.g., see sea level curves of Kelsey et al. (2005); Engelhart et al. (2015); and Dura et al. (2016)). We can crudely estimate how large this effect might be by linearly scaling the change in minimum slip deficit to cause lake inundation to a change in sea level relative to the outlet elevation on the same paleolandscape. For grid C, the landscape with the most landward shoreline, a change of sea level from 2.07 to 1.55 m (NAVD88) increased minimum slip deficit by 10 years for the splay fault source and 20 years for the full-margin symmetric slip source (Table 1). For a sea level 4 m lower 4600 years ago, this increase scales to 80 and 155 years peak slip deficit (3–5 m slip) for the splay fault and symmetric slip sources, respectively. This additional slip deficit at ~ 4600 years ago would increase the Witter et al. (2012) minimum slips for grid C at the latitude of Bradley Lake to 11 and 14 m for the splay fault and symmetric slip cases, respectively. Assuming that a similar increase would occur for the grid B shoreline, the equivalent 12 and 13 m (Table 1) minimums would increase to 15 and 18 m. This change would be equivalent to raising the thresholds on Fig. 7a, b such that the T10 would not necessarily inundate the lake, consistent with its correlation to the lake disturbance event DE14 rather than a tsunami deposit (Fig. 7a).

6.4 Implications for probabilistic tsunami hazard analysis

Our experimental results and the related tsunami simulations of Witter et al. (2012) and Priest et al. (2014) provide useful guidance for construction of a probabilistic tsunami hazard analysis (PTHA) of the CSZ and other subduction zones. For example, this study and Priest et al. (2010, 2014) demonstrate that, when simulating inundation from a local subduction zone earthquake, vertical coseismic deformation immediately offshore is the most important control on maximum wave height and inundation. Priest et al. (2014) found that wave height falls off dramatically more than ~ 70 km north of southern Cascadia ruptures. If assessing a range of peak wave heights is the focus of a PTHA of local subduction zone sources, then it is inefficient to spend computational resources on

simulation of variations in coseismic deformations more than ~ 70 km along strike from a site of interest.

Construction of an array of sources of local tsunamis for a PTHA must take into account available slip deficit on the subduction zone. Priest et al. (2010) found that peak slip on CSZ sources is nearly linearly correlated with peak tsunami wave height at the open coast for any given slip distribution. Peak slip in the CSZ probably approximates tectonic slip deficit from plate convergence. Peak slips for an array of sources for a PTHA must therefore fit within reasonable limits of potential peak slip deficit that can be released given the local convergence rate and taking into account qualitative and quantitative paleoseismic clues to the range and frequencies of potential peak slips. Judging reasonable limits on peak slip is complex but should take into account maximum inter-seismic intervals from the geological record, minimum slip to produce documented tsunami inundations, and total available slip and seismic energy storage on the subduction zone. In our study of the CSZ, there is little slip beyond the minimum to account for known tsunami inundations and turbidites over the last ~ 4700 years.

Variations in slip distribution up and down dip on the subduction zone are important for seismic hazard analysis but less so for PTHA. Priest et al. (2010) and Witter et al. (2013, 2012) demonstrated that geologically reasonable variations in slip distribution make little difference in tsunami wave height or inundation unless significant slip is partitioned from the megathrust to a master splay fault. Therefore, every PTHA logic tree should include the effect of splay faults, if present. An exception to these generalizations is the possibility of unusually large slip within the outermost part of the accretionary wedge as apparently occurred in the 2011 Tohoku earthquake (Tsuji et al. 2013). In this case the assumption of velocity strengthening behavior in all of our fault models breaks down. Priest et al. (2014) argue that such an event may be possible in southern Cascadia where the Pleistocene accretionary wedge is thin and continental slope steep, but only for rare, unusually large releases of slip approaching the ~ 50 – 60 m of the Tohoku earthquake.

Finally, it is useful to ask whether a Cascadia PTHA would produce the minimum peak slips for lake inundation if the analysis took into account only the turbidite-estimated rupture lengths of Goldfinger et al. (2013a) and global seismic data for subduction zones. Using the Scholz (1982) global ratio of mean slip to length (2×10^{-5}), Table 4 lists predicted mean and peak slips for all of the Goldfinger (2013a) rupture lengths of Fig. 1a. Peak slip is assumed to equal ~ 1.6 times mean slip based on the ratio at Bradley Lake ($\sim 43^\circ\text{N}$) in Table 1 from Witter et al. (2012). This approach yields estimated peak slips for all C' and longer ruptures that are large enough (>8 – 13 m) to inundate Bradley Lake from ruptures immediately offshore (Table 1), consistent with the paleoseismic observations that most ruptures this long produced lake inundation (Table 3). This approach also correctly predicts that Segment D ruptures would not likely produce lake inundation, because all fall below the minimum of 15 – 22 m peak slip needed to inundate the Lake (Table 2).

One caveat is that there is no attempt in this rupture length approach to create an array of sources with slip summing to the plate convergence rate. Clearly, every one of the nine full-margin ruptures recorded as sandy turbidites deposited since T10 at ~ 4700 years (Table 3; Fig. 7a) could not have had 33 m peak slip (Table 4), because the resulting total slip of ~ 300 m exceeds the ~ 150 m available from plate convergence at ~ 32 mm/yr.

Slip could be balanced by estimating the variation in slip within each length category. Such variation is probably responsible for the wide range in sandy turbidite mass noted by Goldfinger et al. (2012) and used by Rong et al. (2014) to estimate variation in magnitude of CSZ earthquakes. North to south slip taper required by the seismic energy balance

Table 4 CSZ fault slip predicted by turbidite-derived fault rupture lengths (Fig. 1a), assuming the Scholz (1982) ratio of slip to length of 2×10^{-5}

Segment (Goldfinger et al. 2013a)	Length (km)	Mean slip (m)	Peak slip (m) ^a
Full margin	1000	20	33
B (upper limit)	860	17	28
B (best estimate)	790	16	26
B (lower limit)	720	14	24
C (upper limit)	650	13	21
C (best estimate)	615	12	20
C (lower limit)	580	12	19
C' upper limit	540	11	18
C' (best estimate)	485	10	16
C' (lower limit)	425	9	14
D (upper limit)	400	8	13
D (best estimate)	310	6	10
D (lower limit)	230	5	7

^a Peak slip = $1.6 \times$ mean slip based on the ratio of these peak to mean slip in Witter et al. (2012) and Table 1

calculations of Scholz (2014) is another factor that could be integrated into a PTHA to achieve approximate slip balance. For example, Scholz (2014) estimates a ~ 50 percent reduction in slip on full-margin ruptures from Washington to the latitude of Hydrate Ridge. Likewise, recognition that some relatively long ruptures like T2, T5a, T5b, and T5c that produce little or no evidence of tsunami inundation can be factored into the logic tree weights of a PTHA.

7 Conclusions

A key finding of this study is that tsunamis generated by southernmost Cascadia ruptures like the Segment D of Goldfinger et al. (2012) are unlikely to deposit tsunami sediments in Bradley Lake, because slip and resulting vertical coseismic deformation from this source (Fig. 4) is generally concentrated too far south of the lake to efficiently project tsunami energy into the lake. Minimum slip deficit release of 430–640 years (15–22 m peak coseismic slip) on the megathrust south of Cape Blanco is necessary to produce tsunamis that breach the 6-m lake outlet barrier for the most likely paleolandscapes and tides. Frequent release of slip deficits as large as 640 years on the southern part of the megathrust is inconsistent with the ~ 300 -km length in that part of the CSZ or possible slip budgets over the last ~ 4700 years. When Hydrate Ridge data are utilized, up to 8 of the last 12 (67%) inter-turbidite times are consistent with tsunami inundations of Bradley Lake versus 4 of the last 12 (33%) when, as shown by Witter et al. (2012), a similar analysis is done for Rogue Apron data. The four inundations not predicted by the Hydrate Ridge inter-turbidite time data and lack of correspondence of some turbidites there to either inundations or lake disturbances at Bradley Lake verify the conclusion of Witter et al. (2012) that inter-event times are not reliable predictors of coseismic slip, possibly because (1) slip deficit is stored

over many earthquake cycles before being released; and/or (2) there was insufficient slip to produce large tsunamis during some ruptures that triggered turbidites offshore.

We also demonstrate that there is relatively little slip deficit available from plate convergence over the last ~4700 years to account for tsunamis that may have been higher than the minimums to cause lake inundation or for earthquakes larger than the minimum to trigger turbidites without lake inundation. Using minimal coseismic slip assigned to non-inundating events recorded as turbidites at Hydrate Ridge and enough slip to cause lake inundation across the more seaward (AD1700) shoreline results in over estimation of available slip deficit, although an under estimation is also possible when using the most landward shoreline. Nevertheless, the minimum slip values to cause lake inundation overlap mean slip estimated independently by Scholz (2014) from an analysis of seismic energy balance for this part of the Cascadia subduction zone. The tendency for the inter-event method for slip estimation to overestimate cumulative slip can probably be traced to inherent shortcomings of the fault dislocation and tsunami simulations in emulating nature. Further direct observations of modern subduction zone earthquakes and tsunamis combined with detailed paleoseismic investigations will offer crucial constraints on development of more accurate source models for tsunami generation.

This experiment and related previous work of Witter et al. (2012) and Priest et al. (2014) can be synthesized into general guidance for integration of global seismic observations with paleoseismic data into a PTHA. For example, a PTHA based only on turbidite-defined CSZ rupture lengths and the Scholz (1982) global ratio of mean slip to length would yield an array of tsunami scenarios broadly consistent with the Bradley Lake inundations over the last ~4600 years; albeit balancing total slip to available slip deficit from plate convergence would still be a challenge.

Acknowledgements This investigation was supported by the Oregon Department of Geology and Mineral Industries. Computational facilities at the College of William and Mary which were provided with the assistance of the National Science Foundation, the Virginia Port Authority, and Virginia's Commonwealth Technology Research Fund, and also using the Extreme Science and Engineering Discovery Environment (XSEDE; Grant #TG-CCR120029), which is supported by National Science Foundation grant number OCI-1053575.

References

- Adams J (1990) Paleoseismicity of the Cascadia subduction zone—evidence from turbidites off the Oregon–Washington margin. *Tectonics* 9:569–583
- Atwater BF, Hemphill-Haley E (1997) Recurrence intervals for great earthquakes of the past 3,500 years at northeastern Willapa Bay, Washington. US Geol Surv Prof Paper 1576
- Atwater BF, Carson B, Griggs GB, Johnson HP, Salmi MS (2014) Rethinking turbidite paleoseismology along the Cascadia subduction zone. *Geology*. doi:10.1130/G35902.1
- Bernstein EH (1925) Topography of the Oregon coast south of Coquille River, T-Sheet 4216, 1:20,000 scale, US Natl Geod Surv, Silver Spring
- Black B (2014) Stratigraphic correlation of seismoturbidites and the integration of sediment cores with 3.5 khz chirp subbottom data in southern Cascadia. Masters thesis, Oregon State University
- Blaser L, Krüger F, Ohmberger M, Scherbarum F (2010) Scaling relations of earthquake source parameter estimates with special focus on subduction environment. *Bull Seismol Soc Am* 100(6):2914–2926
- Burgette RJ, Weldon RJ II, Schmidt DA (2009) Inter-seismic uplift rates for western Oregon and along-strike variation in locking on the Cascadia subduction zone. *J Geophys Res* 114(B01408):1–24
- Dura T, Engelhart SE, Vacchi M, Horton BP, Kopp RE, Peltier WR, Bradley S (2016) The role of Holocene relative sea-level change in preserving records of subduction zone earthquakes. *Curr Climate Change Rep* 2(3):86–100

- Engelhart SE, Vacchi M, Horton BP, Nelson AR, Kopp RE (2015) A sea-level database for the Pacific coast of central North America. *Quat Sci Rev* 113:78–92
- Frankel AD (2011) Summary of November 2010 meeting to evaluate turbidite data for constraining the recurrence parameters of great Cascadia earthquakes for the update of the national seismic hazard maps. U.S. Geol Surv Open-File Report 2011–1310, p 13. <http://pubs.usgs.gov/of/2011/1310/>
- Geist EL (1998) Local tsunamis and earthquake source parameters. In: Dmowska R, Saltzman B (ed) *Tsunamigenic earthquakes and their consequences*, *Adv Geophys* 39, pp 2–1–2–16
- Goldfinger C, Nelson CH, Morey AE, Johnson JE, Gutierrez-Pastor J, Eriksson AT, Karabanov E, Patton J, Gracia E, Enkin R, Dallimore A, Dunhill G, Vallier T (2012) Turbidite event history: Methods and implications for Holocene paleoseismicity of the Cascadia subduction zone, USGS Professional Paper 1661-F, Reston, VA, U.S. Geological Survey, p 178, 64 figures
- Goldfinger C, Ikeda Y, Yeats RS, Ren J (2013a) Superquakes and supercycles. *Seismol Res Lett*. doi:10.1785/0220110135
- Goldfinger C, Morey AE, Black B, Beeson J, Nelson CH, Patton J (2013b) Spatially limited mud turbidites on the Cascadia margin: segmented earthquake ruptures? *Nat Haz Earth Syst Sci* 13:1–38. doi:10.5194/nhess-13-1-2013
- Goldfinger C, Galer S, Beeson J, Hamilton T, Black B, Romsos C, Nelson H, Morey A (2016a) The importance of site selection, sediment supply, and hydrodynamics: a case study of submarine paleoseismology on the northern Cascadia margin, Washington USA. *Marine Geol*. doi:10.1016/j.margeo.2016.06.008
- Goldfinger C, Kane T, Beeson J, Romsos C (2016b) Structural definition of the Cascadia locked zone. Oregon State University, Corvallis, OR, USA, Report ATSM2016-1, p 132
- Hughen KA et al (2004) Marine04 marine radiocarbon age calibration, 26–0 ka BP. *Radiocarbon* 46:1059–1086
- Kelsey HM, Witter RC, Hemphill-Haley E (2002) Plate-boundary earthquakes and tsunamis of the past 5,500 yr, Sixes River estuary, southern Oregon. *Geol Soc Am Bull* 114:298–314. doi:10.1130/0016-7606(2002)114<0298:PBEATO>2.0.CO;2
- Kelsey HM, Nelson AR, Hemphill-Haley E, Witter RC (2005) Tsunami history of an Oregon coastal lake reveals a 4,600 yr record of great earthquakes on the Cascadia subduction zone. *Geol Soc Am Bull* 117(7/8):1009–1032
- Komar P (1997) *The Pacific Northwest coast: living with the shores of Oregon and Washington*. Duke University Press, Durham, NC, 195 pp
- Komar PD, Allan JC, Ruggiero P (2011) Sea level variations along the U.S. Pacific Northwest coast: Tectonic and climate controls. *J Coastal Res* 27(5):808–823
- McCaffrey R, King RW, Payne SJ, Lancaster M (2013) Active tectonics of northwestern US inferred from GPS-derived surface velocities. *J Geophys Res Solid Earth* 118(2):709–723
- Milker Y, Nelson AR, Horton BP, Engelhart SE, Bradley LA, Witter RC (2016) Differences in coastal subsidence in southern Oregon (USA) during at least six prehistoric megathrust earthquakes. *Quat Sci Rev* 142:143–163
- Mofjeld HO, Foreman MGG, Ruffman A (1997) West Coast tides during Cascadia subduction zone tsunamis. *Geophys Res Lett* 24(17):2215–2218
- Nelson AR, Jennings AE, Kashima K (1996) An earthquake history derived from stratigraphic and microfossil evidence of relative sea-level change at Coos Bay, southern coastal Oregon. *Geol Soc Am Bull* 108:141–154. doi:10.1130/0016-7606(1996)108<0141:AEHDFS>2.3.CO;2
- Nelson AR, Ota Y, Umitsu M, Kashima K, Matshushima Y (1998) Seismic or hydrodynamic control of rapid late-Holocene sea-level rise in southern coastal Oregon, USA? *Holocene* 8:287–299. doi:10.1191/095968398668600476
- Nelson AR, Kelsey HM, Witter RC (2006) Great earthquakes of variable magnitude at the Cascadia subduction zone. *Quat Res* 65:354–365
- Nelson AR, Sawai Y, Jennings AE, Bradley LA, Gerson L, Sherrod BL, Sabean J, Horton BP (2008) Great-earthquake paleogeodesy and tsunamis of the past 2000 years at Alsea Bay, central Oregon coast, USA. *Quat Sci Rev* 27(7–8):747–768. doi:10.1016/j.quascirev.2008.01.001
- Nicolosky DJ, Suleimani EN, Hansen RA (2013) Note on the 1964 Alaska tsunami generation by horizontal displacements of ocean bottom. Numerical modeling of the runup in Chenega Cove, Alaska. *Pure and Appl Geophys* 170(9):1433–1447
- Okada Y (1985) Surface deformation due to shear and tensile faults in a half-space. *Bull Seismol Soc Am* 75(4):1135–1154
- Priest GR, Goldfinger C, Wang K, Witter RC, Zhang Y, Baptista AM (2010) Confidence levels for tsunami-inundation limits in northern Oregon inferred from a 10,000-year history of great earthquakes at the Cascadia subduction zone. *Nat Hazards*. doi:10.1007/s11069-009-9453-5

- Priest GR, Zhang Y, Witter RC, Wang K, Goldfinger C, Stimely L (2014) Tsunami impact to Washington and northern Oregon from segment ruptures on the southern Cascadia subduction zone. *Nat Hazards*. doi:[10.1007/s11069-014-1041-7](https://doi.org/10.1007/s11069-014-1041-7)
- Petersen MD, Moschetti MP, Powers PM, Mueller CS, Haller KM, Frankel AD, Zeng Y, Rezaeian, S, Harmsen SC, Boyd OS, Field N, Chen R, Rukstales KS, Luco N, Wheeler RL, Williams RA, Olsen AH (2014) Documentation for the 2014 update of the United States national seismic hazard maps. U.S. Geol Surv Open-File Report 2014–1091, p 243. doi:[10.3133/ofr20141091](https://doi.org/10.3133/ofr20141091)
- Reimer PJ et al (2004) IntCal04 terrestrial radiocarbon age calibration, 26–0 ka BP. *Radiocarbon* 46:1029–1058
- Rodríguez-Pérez Q, Ottemöller L (2013) Finite-fault scaling relations in Mexico. *Geophys J Int* 193:1570–1588
- Rong Y, Jackson DD, Magistrale H, Goldfinger C (2014) Magnitude limits of subduction zone earthquakes. *Bull Seismol Soc Am*. doi:[10.1785/0120130287](https://doi.org/10.1785/0120130287)
- Satake K, Wang K, Atwater BF (2003) Fault slip and seismic moment of the 1700 Cascadia earthquake inferred from Japanese tsunami descriptions. *J Geophys Res* 108(B11):2535. doi:[10.1029/2003JB002521](https://doi.org/10.1029/2003JB002521)
- Scholz CH (1982) Scaling laws for large earthquakes: consequences for physical models. *Bull Seismol Soc Amer* 72(1):1–14
- Scholz CH (2014) Holocene earthquake history of Cascadia: a quantitative test. *Bull Seismol Soc Am* 104(4):2120–2124
- Scholz CH, Campos J (2012) The seismic coupling of subduction zones revisited. *J Geophys Res*. doi:[10.1029/2011JB009003](https://doi.org/10.1029/2011JB009003)
- Shi B, Brune JN (2005) Characteristics of near-fault ground motions by dynamic thrust faulting: two-dimensional lattice particle approaches. *Bull Seismol Soc Amer* 95(6):2525–2533
- Shimazaki K, Nakata T (1980) Time-predictable recurrence model of large earthquakes. *Geophys Res Lett* 7:279–282
- Sieh K et al (2008) Earthquake supercycles inferred from sea-level changes recorded in the corals of West Sumatra. *Science* 322:1674–1678
- Stuiver M, Reimer PJ (1993) Extended 14C data base and revised CALIB 3.0 14C age calibration programme. *Radiocarbon* 35(1):215–231
- Titov VV, Synolakis CE (1997) Extreme inundation flows during the Hokkaido-Nansei-Oki tsunami. *Geophys Res Lett* 24(11):1315–1318
- Tsuji T, Kawamura K, Kanamatsu T, Kasaya T, Fujikura K, Ito Y, Tsuru T, Kinoshita M (2013) Extension of continental crust by anelastic deformation during the 2011 Tohoku-oki earthquake: the role of extensional faulting in the generation of a great tsunami. *Earth Planet Sci Lett* 364:44–58
- Wang K, He J (2008) Effects of frictional behaviour and geometry of subduction fault on coseismic seafloor deformation. *Bull Seismol Soc Am* 98(2):571–579
- Witter RC, Kelsey HM, Hemphill-Haley E (2003) Great Cascadia earthquakes and tsunamis of the past 6700 years, Coquille River estuary, southern coastal Oregon. *Geol Soc Am Bull* 115:1289–1306
- Witter RC, Zhang YJ, Wang K, Priest GR, Goldfinger C, Stimely L, English JT, Ferro PA (2011) Simulating tsunami inundation at Bandon, Coos County, Oregon, using hypothetical Cascadia and Alaska earthquake scenarios. *Oreg Dep Geol Min Indus Special Paper* 43
- Witter RC, Zhang Y, Wang K, Goldfinger C, Priest GR, Allan JC (2012) Coseismic slip on the southern Cascadia megathrust implied by tsunami deposits in an Oregon lake and earthquake-triggered marine turbidites. *J Geophys Res*. doi:[10.1029/2012JB009404](https://doi.org/10.1029/2012JB009404)
- Witter RC, Zhang YJ, Wang K, Priest GR, Goldfinger C, Stimely L, English JT, Ferro PA (2013) Simulated tsunami inundation for a range of Cascadia megathrust earthquake scenarios at Bandon, Oregon, USA. *Geosphere* 9:1783–1803. doi:[10.1130/GES00899.1](https://doi.org/10.1130/GES00899.1)
- Zhang Y (2012) SELFIE. In: Proceedings and results of the 2011 NTHMP model benchmarking workshop, National Tsunami Hazard Mitigation Program, pp 303–336. <http://nws.weather.gov/nthmp/documents/nthmpWorkshopProcMerged.pdf>. Accessed 18 Jan 2015
- Zhang Y, Baptista AM (2008) An efficient and robust tsunami model on unstructured grids Part I: inundation benchmarks. *Pure appl Geophys* 165(11–12):2229–2248. doi:[10.1007/s00024-008-0424-7](https://doi.org/10.1007/s00024-008-0424-7)
- Zhang Y, Witter RW, Priest GP (2011) Tsunami–tide interaction in 1964 Prince William Sound tsunami. *Ocean Model* 40:246–259
- Zhang Y, Priest GR, Allan J, Stimely L (2016a) Benchmarking an unstructured-grid model for tsunami current modeling. *Pure Appl Geophys*. doi:[10.1007/s00024-016-1328-6](https://doi.org/10.1007/s00024-016-1328-6)
- Zhang YJ, Ye F, Stanev EV, Grashorn S (2016b) Seamless cross-scale modelling with SCHISM. *Ocean Model* 102:64–81

Zilkoski DB., Richards JH, Young GM (1992) Results of the general adjustment of the North American Vertical Datum of 1988. American Congress on Surveying and Mapping, Surveying and Land Information Systems 52(3):133–149, http://www.ngs.noaa.gov/PUBS_LIB/NAVD88/navd88report.htm. Accessed 25 March 2013